coatings

MDPI

Article

Characterization of Hydroxyapatite (HA) Sputtering Targets by APS Methods

Kuo-Yung Hung [1,*], Hong-Chen Lai [2], Yung-Chin Yang [3] and Hui-Ping Feng [1]

1 Department of Mechanical Engineering, Ming Chi University of Technology, New Taipei City 24301, Taiwan; hpfeng@mail.mcut.edu.tw
2 Institute of Mechanical and Electrical Engineering, Ming Chi University of Technology, New Taipei City 24301, Taiwan; jasontuba@gmail.com
3 Institute of Materials Science and Engineering, National Taipei University of Technology, Taipei 10608, Taiwan; ycyang@ntut.edu.tw
* Correspondence: kuoyung@mail.mcut.edu.tw; Tel.: +88-62-2908-9899 (ext. 4514)

Academic Editors: James Kit-hon Tsoi and Krasimir Vasilev
Received: 29 June 2017; Accepted: 7 November 2017; Published: 11 November 2017

Abstract: Radio frequency (RF) sputtering is a potential medical device coating technology that is commercializable; however, a suitable commercialized target for sputtering the hydroxyapatite (HA) coating onto titanium medical devices is more important. Therefore, this study used three HA targets in conducting sputtering experiments for HA films, which were manufactured in a laboratory by using three different processes: cold pressing and sintering (CPS), hot isostatic pressing (HIP), and atmospheric plasma spraying (APS). Subsequently, the sputtering performance of each type of target and the properties of the HA films were assessed to develop an appropriate process for modifying the surfaces of medical devices. The experimental results showed that the APS target, with a density of approximately 2.83 g/cm^3, was suitable for use in HA sputtering. Additionally, the APS target could withstand a high discharge power over 300 W, whereas the CPS target could nearly endure a power below 70 W. The APS target, with Ca/P ratio of 2.401, consisted of a combination of HA, α-tricalcium phosphate (α-TCP), β-TCP, and tetracalcium phosphate phases (TTCP). In addition to being able to perform at a high sputtering power of more than 300 W, the APS target achieved a higher deposition rate than did the CPS target. This study shows that the processing technology used for the APS target is a potential method for applying HA sputtering for the surface modification of artificial aggregates.

Keywords: hydroxyapatite; sputtering target; medical device; atmospheric plasma spraying

1. Introduction

Hydroxyapatite (HA, $Ca_{10}(PO_4)_6(OH)_2$), also referred to as biological apatite, has a similar composition to human bones, exhibits excellent bioactivity, and is crucial for the tissue/implant osseointegration process used in manufacturing medical devices, such as fusion cages, implants for dental roots, and hip joints [1–4]. HA plasma spraying [5–8] is one of the available surface modification techniques for dental roots and hip joints. Regarding HA plasma spraying, a plasma spraying gun is expensive, and plasma-sprayed HA coatings, which are typically 50–250 μm in thickness [7], might contain non-crystalline phases and voids that can easily lead to disintegration between HA films and aggregates, because the coating is susceptible to degradation in human body fluid.

Sputter-deposited HA thin film [9–17] exhibits favorable uniformity and does not easily fall off the bone material because of the high adhesion strength between the aggregates and the film. Studies concerning HA-sputtered titanium implant surface modifications have been reported for producing the HA targets, such as cold pressing and sintering (CPS) [18,19] and hot isostatic pressing (HIP) [18]. Thus, this study was undertaken to conduct sputtering experiments for HA films by using two HA

targets (CPS and HIP targets) with copper backs that were produced in a laboratory. The HA target fabricated using the HIP technique led to cracks on the target due to the existence of residual stress induced during the high-temperature processing (1200 °C). The maximum power of sputtering HA by a CPS target is only about 90 W, resulting in low sputtering rate [18].

The objective of this paper is to develop a novel HA target process that could sustain long-term sputtering processes on high power (>250 W) and not be broken during the bombardment process. The considered technology, atmospheric plasma spraying (APS), has characteristics of high deposition speed and allows the building of thick and dense deposits of high melting temperature materials. It is then suitable for the manufacture of high-stability HA target technology. Subsequently, this study assessed the sputtering performance of the targets and the properties of the HA films to establish an appropriate process for HA sputtering targets, thus enabling the surfaces of SLA-like implants to be modified. SLA-like is a surface modification technology for dental implants, similar to Straumann Company's SLA. The SLA process comprises sand blasting with a large grit (250–500 μm) and acid-etched (SLA) implants by using both sulfuric and hydrochloric acid. This process results in a specific surface roughness on titanium after the SLA process. We call it "SLA-like" because the process is the same as SLA (sand blasting and acid etching) but the experimental parameters—for example, the concentration of acid, reaction time, reaction temperature, and surface roughness—are different. The entire surface of the implant has uniform micrometer-to nanometer-sized holes in it. Most researchers were unaware of the correct and detailed parameters of the Straumann Company's product.

2. Materials and Methods

2.1. Manufacture of the Hydroxyapatite Target

In this study, sputtering experiments were conducted on the HA, which were produced using three targets, each with a diameter of two inches, and were fabricated using CPS (Table 1), HIP (Table 2), and APS (Table 3). A commercially-available HA powder (Sigma-Aldrich H0252, St. Louis, MO, USA) was used as the target material in the CPS and HIP processes, because it compacts easily and has a large particle size of approximately 100 μm. An HA powder (XPT-D-703, Sulzer Metco, New York, NY, USA), with a fine particle size of approximately 30 μm, was used as the target in the APS process, because this HA powder enables easy powder-feed flowing. The target used in the APS process was manufactured by plasma spraying HA powder directly onto a copper backing plate (Figure 1). Conversely, the HA compacts that were used for the sintered targets (used in the HIP and CPS processes) were bonded to a copper backing plate by using silver-loaded epoxy resin and then, to complete the preparation of these two targets, the compacts were cured at 250 °C for 30 min in air under a pressing load of 10 kg (Figure 2).

Table 1. Processing parameters for the HIP target [18].

Process	Parameter
Powder	SIGMA Sigma-Aldrich H0252
Sintering Temperature	1100 °C
Post Heat Treatment	1000 °C at a set time of 2 h
Cooling	Naturally in furnace
Adhesion Glue	AB type Ag glue
Target Thickness	2 mm
Target Size	2 inches in diameter

Table 2. Processing parameters for the cold pressing and sintering (CPS) target [18].

Process	Parameter
Powder	SIGMA Sigma-Aldrich H0252
Press Type	Hydraulically pressing
Sintering Furnace	Tube type
Sintering Temperature	1050 °C in air environment
Heating Rate	3 °C/min
Sintering Duration	2 h
Cooling	naturally in furnace
Adhesion Glue	AB type Ag glue
Target Thickness	2 mm
Target Size	2 inches in diameter

Table 3. Processing parameters for the APS target [19].

Process	Parameter
Powder	Sulzer Metco XPT-D-703
Environment	In air
Flow Rate of Primary Gas (Ar)	50 L/min
Flow Rate of Secondary Gas (H_2)	14 L/min
Torch Current	660 A
Power	47.9 kW
Stand-off Distance	7.5 cm
Surface Speed	150 rpm
Transverse Speed	5 mm/s
Flow Rate of Powder Carrier Gas (Ar)	3 L/min
Powder Feed Rate	10 rpm
Spraying Loop	120
Voltage	72.5 V
Target Thickness	2 mm
Target Size	2 inches in diameter

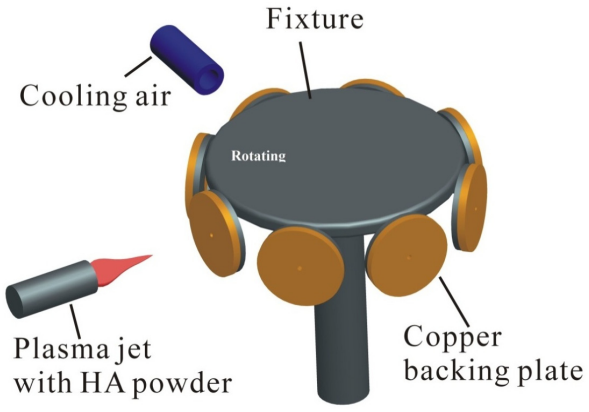

Figure 1. Schematic representation of the atmospheric plasma spraying (APS) target manufactured directly by plasma spraying hydroxyapatite (HA) powder onto a copper backing plate.

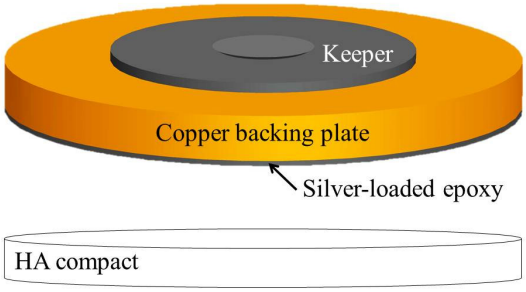

Figure 2. Schematic representation of the sputtering HA targets for CPS and hot isostatic pressing (HIP) targets.

2.2. Sputtering Procedure and Characterization of the Hydroxyapatite Films

Figure 3 shows a flowchart of this study. The processing parameters for the three HA targets and sputtering conditions for the HA thin films were set based on previous studies [18,19]. All samples of the HA films were deposited using an RF sputter (Kao-Duen R25A08, New Taipei City, Taiwan) onto 99.9999% pure silicon wafer substrates, each containing a target from each of the three types (CPS, HIP, and APS), at a discharge power of 50–300 W (run at the set processing parameters, as shown in Table 5). The HA powders and HA films with each of the three targets were characterized using Fourier transform infrared spectroscopy (Fourier transform infrared spectroscope, FTIR, One FT-IR, Perkin Elmer, Waltham, MA, USA; frequency range 4000–400 cm^{-1}, resolution 8 cm^{-1}) and energy dispersive X-ray analysis (energy-dispersive X-ray spectroscope, EDS, S-3400N, HITACHI, Tokyo, Japan) according to the phase structure contents, molecular group contents, and Ca/P ratio calculation. The X-ray diffraction patterns were measured using a Rigaku Multiplex Diffractometer (Rigaku, Tokyo, Japan). The Rietveld-refinement analysis (with the HighScore Plus software, Version 4.7) was employed to determine phases and ceramic crystallinities. Grain morphologies and Ca/P ratios of elements were obtained by using a scanning electron microscope (SEM, JSM-6701F, JEOL, Tokyo, Japan) equipped with energy-dispersive X-ray spectroscopy (EDS). Film thickness was measured using a scanning electron microscope (FE-SEM, JSM-6701F, JEOL, Tokyo, Japan). Thermal expansion was analyzed using a push-rod dilatometer (Netzsch DIL 402 C, Netzsch, Selb, Germany).

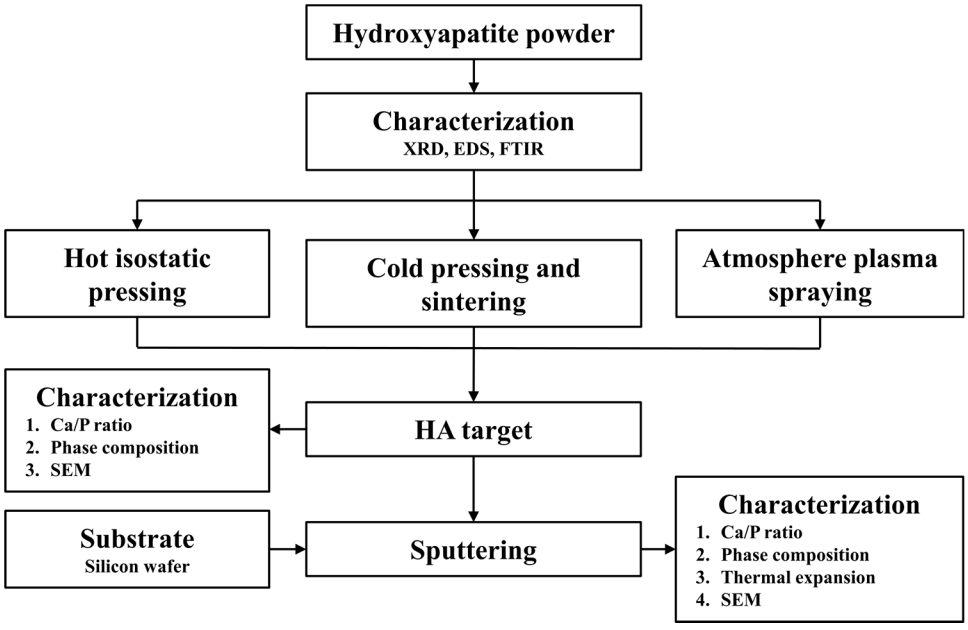

Figure 3. Flowchart of this study.

3. Results and Discussion

3.1. Characterization of the Hydroxyapatite Powders

The peaks of the HA phase in the XRD patterns of two HA powders, which were obtained from Sigma-Aldrich and Sulzer Metco (Figure 4), indicating that both of the powders exhibited a single phase and fully-crystalline HA structures, but the XRD phase peaks that were obtained from the Sulzer Metco powder were higher than those of the Sigma-Aldrich powder. The FTIR spectra (Figure 5) show that both of the HA powders exhibited molecular groups associated with OH^- and PO_4^{3-} bands, but a small quantity of the carbonate ion group (CO_3^{2-}) in the Sigma-Aldrich powder was incorporated into the HA phase. The results of the XRD analysis indicated that the Sigma-Aldrich powder exhibited a trace of the secondary species of the carbonate group, and the Sulzer Metco powder exhibited a single-phase HA structure.

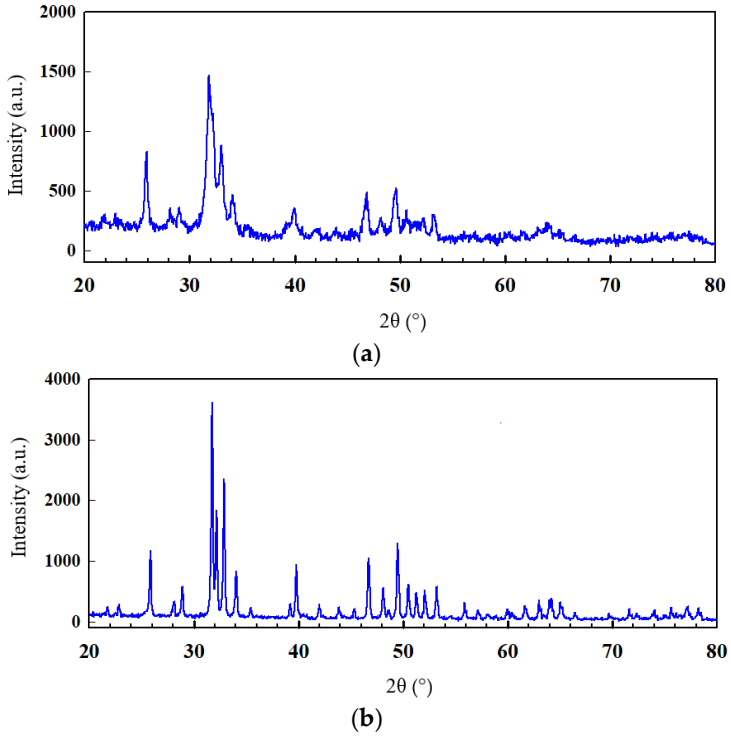

Figure 4. XRD patterns of HA powders obtained from: (**a**) Sigma, and (**b**) Sulzer Metco. ICSD (International Center for Diffraction Data): HA 98-001-2623.

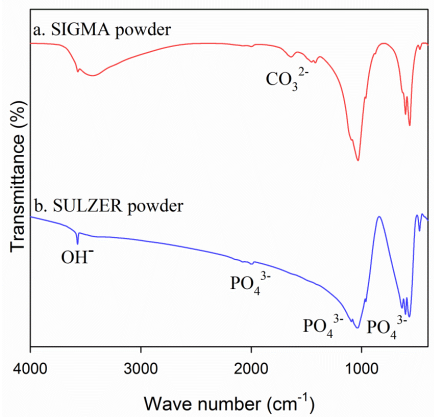

Figure 5. FTIR spectra of HA powders obtained from: (**a**) Sigma and (**b**) Sulzer Metco.

3.2. Characterization of the Hydroxyapatite Targets

3.2.1. Phase and Composition

The XRD (Figure 6) and EDS (Table 4) of the three HA targets show that the HIP target with a Ca/P ratio of 1.679 and the CPS target with a Ca/P ratio of 2.04 contained a similar HA phase structure. In contrast to the XRD analysis, the crystalline phase of calcium phosphate in the APS target was lower than the HIP and CPS targets (Figure 6a,b). Hence, the crystallinity of the HA material on the APS target was lower than the HIP or CPS targets. The HA powder obtained from Sulzer Metco was plasma-sprayed onto a copper backing plate to form the target (called APS) with a Ca/P ratio of 2.401 and a lower crystallinity degree than that of the as-received HA powder from Sulzer Metco. The sharp peaks of the HA phase in the XRD pattern library revealed that the main phase is purely HA (Figure 4). Figure 6b shows X-ray diffraction patterns and Rietveld refinements with various phases (HA, TCP and TTCP) and crystallinities. The accuracy criteria of goodness-of-fit (γ^2) is required to be less than 2. The Rietveld refinements confirm a predominant HA phase in all ceramic targets. The crystallinity is defined by the intensity ratio of the diffraction peaks and of the sum of all measured intensity, i.e., crystallinity (%) = $100 \times \sum I_{net}/(\sum I_{tot} - \sum_{background})$. The crystallinities are about 59.4%, 56.0%, and 37.4% for CPS, HIP, and APS ceramic targets, respectively. However, the XRD of the target shows that the crystallinity of the APS target is the lowest. By contrast, the Ca/P of the thin-film could be controlled by different sputtering powers on the APS target. The target was transformed, exhibiting a combination of various phases, such as crystalline and amorphous HA, tricalcium phosphate (α-TCP, β-TCP), and tetracalcium phosphate (TTCP). When the temperature is as high as 800 °C, the hydroxyapatite undergoes a nonhydroxylation reaction. When the temperature is as high as 1050 °C, HA would degrade to β-TCP and TTCP. If the temperature is as high as 1120 °C, β-TCP would transform to α-TCP [5,20,21]. In Figure 6b, the insets are SEM grain morphologies with Ca/P ratios from the cross-sections of as-sintered ceramic targets. It shows that CPS and HIP had similar grain size and APS's grain size was much larger (So no grain size in the third image of Figure 6b).

The HIP target was a solid target and exhibited a satisfactory phase purity, as well as a density close to the theoretical density of 3.1 g/cm^3, because the HIP compact was manufactured and heat-treated inside a closed steel mold under a certain high pressure and temperature in an argon environment. However, an increased Ca/P ratio was observed in both the CPS and APS targets; this increase may have been due to the evaporation of the phosphate group (PO_4) during the high-temperature fabrication process conducted in air.

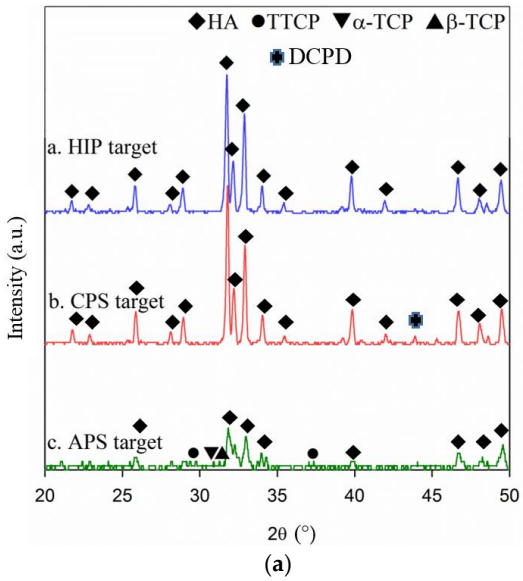

(**a**)

Figure 6. *Cont.*

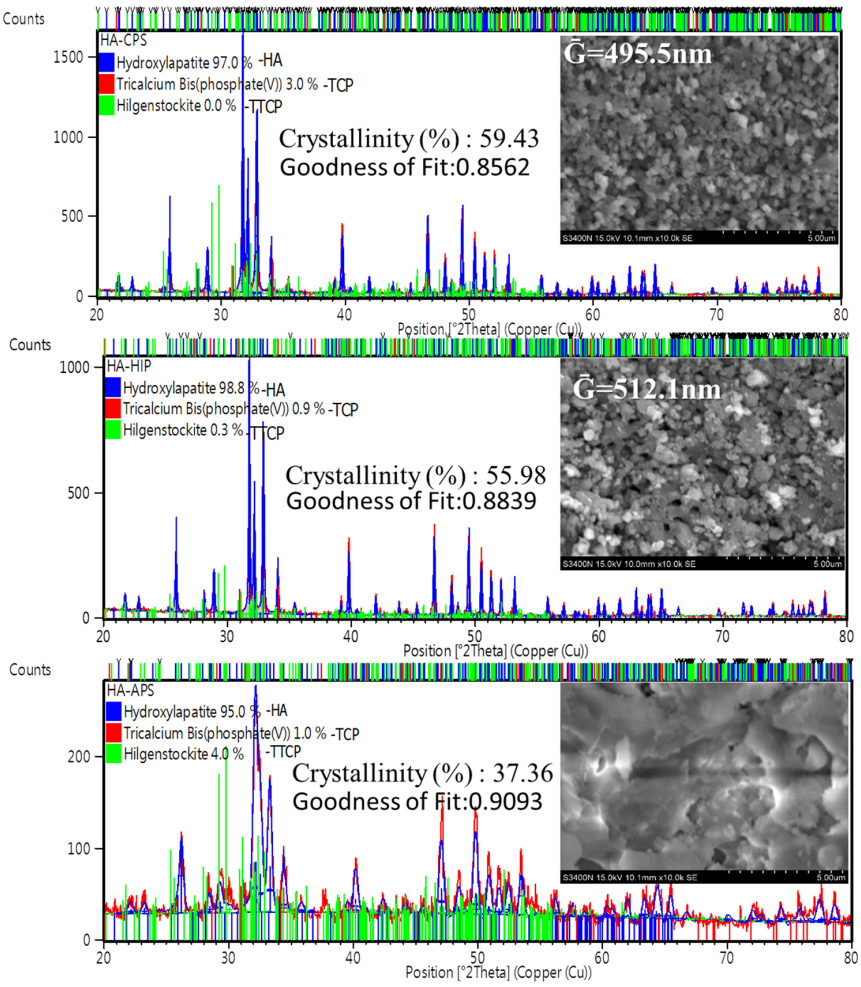

(**b**)

Figure 6. (**a**) XRD plot of the HA targets: HIP, CPS and APS. (ICSD (International Center for Diffraction Data): HA 98-001-2623; tetracalcium phosphate (TTCP) 98-000-6142; α- tricalcium phosphate (TCP) 98-004-2597; β-TCP 98-007-6561; Dicalcium Phosphate Dihydrate (DCPD) 98-000-4706). (**b**) X-ray diffraction patterns and Rietveld refinements of as-sintered ceramic targets (CPS, HIP, and APS). γ^2 is the goodness-of-fit of refinement. Three different phases (HA, TCP and TTCP) were identified as indicated in different colors. The insets are SEM grain morphologies with Ca/P ratios from the cross-sections of as-sintered ceramic targets.

Table 4. EDS results of the HA targets by HIP, CPS and APS.

Target	Element	*k*-Ratio	ZAF	at.%	Ca/P Ratio
HIP	P	0.3345	1.077	36.01	1.679
	Ca	0.5737	1.053	60.41	
CPS	P	0.2792	1.073	29.94	2.04
	Ca	0.6663	1.043	61.07	
APS	P	0.2166	1.076	24.71	2.401
	Ca	0.7427	1.033	59.33	

3.2.2. The Performance of Hydroxyapatite Targets

This study employed three HA targets that were fabricated using the HIP, CPS, and APS processes and used in sputtering HA films on silicon substrates. The sputtering conditions and parameters were set as listed in Table 5 to assess the performance of these targets during the sputtering process. The results showed that the HA target, which was manufactured using the HIP technique, exhibited a high density of 3.1 g/cm^3, close to the theoretical density for HA material (3.16 g/cm^3), which led to the presence of the cracks, even at a low power of 50 W after sputtering (Figure 7a), partly because 3× internal residual stress was induced during the HIP process at a temperature of 1100 °C (higher than the phase transition temperature of 1050 °C of β-TCP, so phase decomposition occurs), and partly because the cracks that originated during the sputtering process arose because of thermal expansion of the CaP (Figure 7a). During the sputtering process, the plasma bombardment on the surface of the target produced high temperatures, and the copper backing plate contact with cooling water forms the low temperature interface. Thus, thermal expansion mismatch between the HA compact and the copper backing plate during the sputtering process probably occurred. Figure 8 shows the thermal expansion and ramping temperature for the three HA targets. Although the CPS target rapidly shrank at temperatures over 1000 °C, it exhibited no breakages (Figure 7b) when sputtering was conducted at a power below 70 W, possibly because the material has a high porosity and low density (1.43 g/cm^3), which alleviated stress and prevented cracking. However, the CPS target could not withstand a power higher than 70 W. This effect can be attributed to the low strength and density of the compact. The APS target exhibited nearly no change in dimensions (Figure 7c) and withstood a sputtering power of up to 300 W without any breakages occurring. This result might be related to the low porosity and density (2.83 g/cm^3) of the APS target, which balanced the thermal expansion. Besides this, we have checked the decreased thickness of the target as requested. After 1 h of sputtering at 300 W, the average thickness of the APS target decreased approximately 15 μm. The total thickness of the APS target is 2 mm (Table 3). Hence, the target can be used for a long time.

Table 5. Sputtering conditions for HA films.

Process	Parameter
Sputtering Time	60 min
Base Pressure	7.5×10^{-6} torr
Process Pressure	3.0×10^{-3} torr
Ar Flow Rate	20 sccm
Working Distance	70 mm
Power	50–300 W

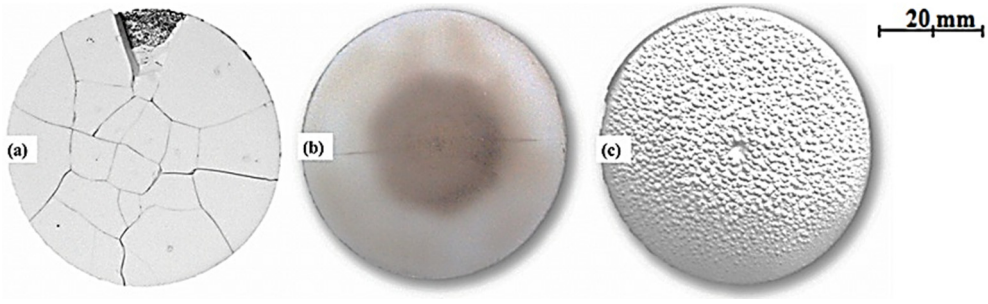

Figure 7. Images of HA targets after sputtering process: (**a**) HIP [18]; (**b**) CPS; and (**c**) APS.

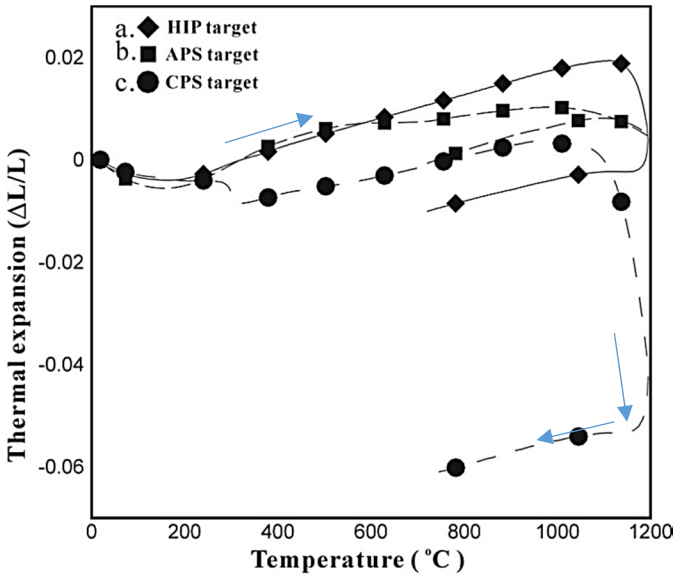

Figure 8. Thermal expansion analysis: (**a**) HIP; (**b**) APS; and (**c**) CPS.

3.3. Characterization of Hydroxyapatite-Sputtered Films

Additionally, because the HIP target breaks at low power, the deposition process is not stable, as the cracked material falls onto the substrate during HA sputtering. Hence, this paper does not deeply discuss the film characteristics of the HIP target. Figure 9 and Table 6, respectively, show the SEM cross-sectional images and Ca/P ratios (determined using EDS) of the HA films sputtered onto silicon substrates by using the CPS and APS targets. Because the silicon substrate is flat enough, it could be used as a good substrate for measuring the thickness of the HA thin-film. When using the CPS target in sputtering at a low discharge power of 70 W for a short endurable duty cycle of 60 min, the film thickness was 34.7 nm, the deposition rate was approximately 0.578 nm/min, and the Ca/P ratio (1.51) differed from that obtained when using the as-received target (2.04). When using the APS target at 300 W for 60 min, the film thickness was 277.6 nm, the deposition rate was approximately 4.62 nm/min, and the Ca/P ratio (2.38) differed from that obtained when using the as-received target (2.401). The decrease in the Ca/P ratio of the HA films sputtered using both CPS and APS targets may be attributed to a higher sputtering yield of atoms (P) with a lower mass and binding energy than those of Ca. Thus, the Ca/P ratio of the HA films is higher than the HA targets.

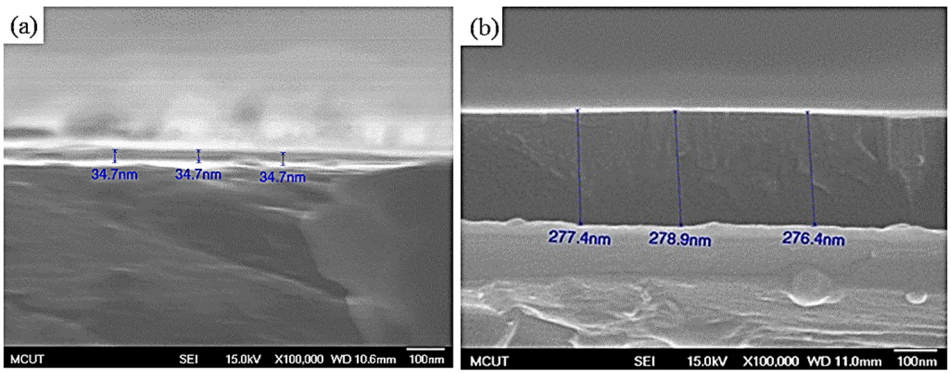

Figure 9. SEM cross-sectional images of as-sputtered HA films onto silicon substrates: (**a**) CPS–70 W–60 min and (**b**) APS–300 W–60 min.

Table 6. EDS results of the HA-sputtered films by CPS–70 W–60 min and APS–300 W–60 min.

Parameter	Element	*k*-Ratio	ZAF	at.%	Ca/P Ratio
CPS Film, 70 W-60 min	P	0.0257	1.735	1.07	1.51
	Ca	0.1003	1.167	1.62	
APS Film, 300 W-60 min	P	0.0317	1.693	5.37	2.38

The XRD patterns of the sputtered HA films (Figure 10) revealed that the film sputtered using the CPS target did not exhibit a crystal structure, whereas the film sputtered using the APS target, of which some peaks can be observed in the XRD plot, was partially crystalline. This was caused by the high temperature that arose because of the high discharge power (300 W) of the APS target, easily facilitating the crystallization of the calcium phosphate material. The distinct peak in Figure 10b indicated that a trace of undesirable $Ca_5(SiO_4)_2CO_3$ was incorporated into the film. This was likely caused by the diffusion of silicon from the silicon substrate into the film. The Ca/P ratio of the film sputtered using the APS target decreased to 2.32, which differed from the stoichiometric value of the HA structure (1.67). This change occurred because amorphous HA appeared in the film. However, this Ca/P ratio and the degree of crystallinity of the HA film may influence the promotion of the biological response within the early healing stage after implantation [5,22–25]. Some studies have claimed that pure HA is the most stable mineral and does not easily degrade in the body; therefore, it can increase the success rate of implants through the use of a thermal spray coating. Schneider [24] and Heimann [25] indicated that the degradation order in the biological environment is CaO >> ACP > α-TCP > β-TCP >> OHA/OA >> HA. Thus, for implantable bone materials with a thermal spray coating (thick film), a pure HA thin film is desirable to avoid degradation and film cracking. By contrast, our thin-film technology is based on the desire to promote the biological response within the early healing stage after implantation, because the long-term success of dental implants largely depends on healing with rapid osseointegration into the bone [26]. Thin films formed through the sputtering of an APS target could result in a different degradation rate for CaP composition, and there would be no cracking issue, as observed in the thick film process. Thus, our thin-film technology that features an APS target can have a healing effect similar to the filling artificial bone powder.

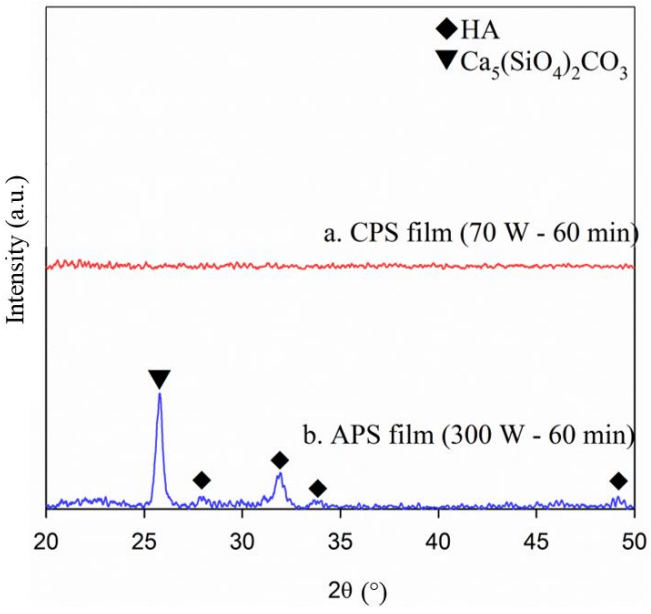

Figure 10. XRD plot of as-sputtered HA films: (**a**) CPS-70W-60 min, and (**b**) APS-300W-60 min.

Although the CPS targets were adopted to run at 70 W for a period of 60 min without breaking, the APS target exhibited a higher density, longer lifetime, higher disposition rate, and higher discharge power limit, as well as enabled fabricating films with a higher relative crystallinity, compared with the CPS target (Figure 10b). After the phase composition was identified through XRD, only the CaP films formed at a higher sputtering power and longer sputtering time revealed HA and monocalcium phosphate anhydrate (MCPA) patterns from the APS target. Thin films formed by sputtering APS target could yield a different degradation rate for CaP composition within the early healing stage after implantation. Because the Ca/P ratio could be controlled by different sputtering power for APS target (Figure 11). The range of the Ca/P ratio could be controlled from 1.47–2.38 by regulating the sputtering power of the APS target. Ca/P ratio (especially Ca/P ~1.67) is one of the most important factors in the biomedical applications of the HA thin films. Even the crystallinity of the APS target is the lowest, but it could suffer a high sputtering power and get a wide range of the Ca/P ratio on HA film. Therefore, the APS process employed in this study can potentially be applied in manufacturing HA targets used for sputtering in the surface modification of medical devices.

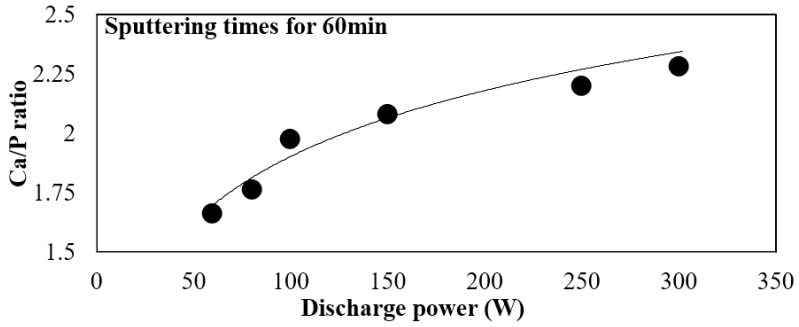

Figure 11. Ca/P ratio of the thin-film at different sputtering power by APS target.

4. Conclusions

This study investigated the performance and properties of three targets that were prepared using CPS, HIP, and APS, and determined a suitable process for fabricating the target for HA-sputtered films. The experimental results revealed that the APS process is a promising method for fabricating HA sputtering targets that exhibit long lifetimes and high deposition rates. Furthermore, the APS target withstood a high discharge power of 300 W during sputtering and facilitated the fabrication of an HA film with crystalline. Conversely, the HIP target was easily broken during sputtering, even at a low sputtering power of 50 W and, therefore, was not suitable. The HIP and the CPS targets exhibited a pure HA phase, whereas the APS target contained a mixed phase of HA, α-TCP, β-TCP, and TTCP, as well as a crystalline and amorphous HA phase. The films sputtered at a power of 70 W by using the CPS target exhibited a thickness of 34.7 nm and were deposited at a rate of about 0.58 nm/min, whereas the films sputtered at a power of 300 W by using the APS target exhibited a thickness of 277.6 nm and were deposited at a rate of about 4.62 nm/min. These results prove that the APS process has the potential to be applied in manufacturing HA targets used for sputtering in the surface modification of medical devices. Because the thin film formed by sputtering of a APS target can yields a different degradation rate for CaP composition (HA, MCPA) within the early healing stage after implantation, it can avoid the collapse of the coated film, such as thick film formation during the thermal spray coating technology. When the phase composition was identified through XRD, only the CaP films at a higher sputtering power and longer sputtering time revealed HA and monocalcium phosphate anhydrate (MCPA) patterns from the APS target. Even the crystallinity of the APS target is the lowest, but it could suffer the highest sputtering power and get a wide range of the Ca/P ratio from 1.47 to 2.38 at different power. Therefore, the APS process employed in this study can potentially be applied in manufacturing HA targets used for sputtering in the surface modification of medical devices.

Acknowledgments: Part of this study was conducted by industry-university cooperative research with Chang Gung Medical (CGM) Technology Co., Ltd. The authors would like to thank CGM for their support with manpower, equipment, and expenditure, which facilitated the smooth progress of the work. Besides, we would like to thanks Chi-Shun Tu, Ping-Yi Chen and Sheng-Fen Wang for the comments of the revised manuscript.

Author Contributions: Kuo-Yung Hung and Hui-Ping Feng conceived and designed the experiments; Yung-Chin Yang helped to realize the plasma spray experiment. Hong-Chen Lai performed the experiments and analyzed the data; and Kuo-Yung Hung and Hui-Ping Feng wrote the paper.

Conflicts of Interest: The authors declare no conflict of interest.

References

1. Bruck, S.D. *Properties of Biomaterials in the Physiological Environment*; CRC Press Inc.: Boca Raton, FL, USA, 1980; p. 142.
2. Hench, L.L.; Ceram, J.A. Bioceramics: From Concept to Clinic. *J. Am. Ceram. Soc.* **1991**, *74*, 1487–1510. [CrossRef]
3. Kühne, J.H.; Bartl, R.; Frisch, B.; Hammer, C.; Jansson, V.; Zimmer, M. Bone formation in coralline hydroxyapatite. Effects of pore size studied in rabbits. *Acta Orthop. Scand.* **1994**, *64*, 246–252. [CrossRef]
4. Deeb, M.E.; Holmes, R.E. Tissue response to facial contour augmentation with dense and porous hydroxyapatite in rhesus monkeys. *J. Oral Maxillofac. Surg.* **1989**, *47*, 1282–1289. [CrossRef]
5. Cizek, J.; Khor, K.A.; Prochazka, Z. Influence of spraying conditions on thermal and velocity properties of plasma sprayed hydroxyapatite. *Mater. Sci. Eng. C* **2007**, *27*, 340–344. [CrossRef]
6. Sun, L.; Berndt, C.C.; Grey, C.P. Phase structural and microstructural investigation of plasma sprayed hydroxyapatite coating. *Mater. Sci. Eng.* **2003**, *360*, 70–84. [CrossRef]
7. Bosco, R.; Beucken, J.V.D.; Leeuwenburgh, S.; Jansen, J. Surface Engineering for Bone Implants: A Trend from Passive to Active Surfaces. *Coatings* **2012**, *2*, 95–119. [CrossRef]
8. Tsui, Y.C.; Doyle, C.; Clyne, T.W. Plasma sprayed hydroxyapatite coatings on titanium substrates Part 1: Mechanical properties and residual stress levels. *Biomaterials* **1998**, *19*, 2015–2029. [CrossRef]
9. Mercioniu, S.; Ciuca, I.; Pasuk, A.; Slav, A.; Morosanu, C.; Bercu, M. Thickness dependence of crystallization process for hydroxyapatite thin films. *J. Optoelectron. Adv. Mater.* **2007**, *9*, 2535–2538.
10. Wolke, J.G.C.; van Dijk, K.; Schaeken, H.G.; de Groot, K.; Jansen, J.A. Study of the surface characteristics of magnetron-sputter calcium phosphate coatings. *J. Biomed. Mater. Res.* **1994**, *27*, 1477–1484. [CrossRef] [PubMed]
11. Wan, T.; Aoki, H.; Hikawa, J.; Lee, J.H. RF-magnetron sputtering technique for producing hydroxyapatite coating film on various substrates. *Biomed. Mater. Eng.* **2007**, *17*, 291–297. [PubMed]
12. Wolke, J.G.C.; Waerden, V.D.; Schaeken, H.G.; Jansen, J.A. In vivo dissolution behavior of various RF magnetron-sputtered Ca-P coatings on roughened titanium implants. *Biomaterials* **2003**, *24*, 2623–2629. [CrossRef]
13. Massaro, C.; Baker, M.A.; Cosentino, F.; Ramires, P.A.; Klose, S.; Milella, E. Surface and biological evaluation of hydroxyapatite-based coatings on titanium deposited by different techniques. *J. Biomed. Mater. Res.* **2001**, *58*, 651–657. [CrossRef] [PubMed]
14. Ding, S.J. Properties and immersion behavior of magnetron-sputtered multi-layered hydroxyapatite/titanium composite coatings. *Biomaterials* **2003**, *27*, 4233–4238. [CrossRef]
15. Aronov, A.M.; Pichugin, V.F.; Eshenko, E.V.; Ryabtseva, M.A.; Surmenev, R.A.; Tverdokhlebov, S.I.; Shesterikov, E.V. Thin calcium-phosphate coating produced by RF-magnetron sputtered and prospects for their use in biomedical engineering. *Biomed. Eng.* **2008**, *42*, 123–127. [CrossRef]
16. Verestiuca, L.; Morosanub, C.; Bercuc, M.; Pasuik, I.; Mihailescu, I.N. Chemical growth of calcium phosphate layers on magnetron sputtered HA films. *J. Cryst. Growth* **2004**, *264*, 483–491. [CrossRef]
17. Narushima, T.; Ueda, K.; Goto, T.; Masumoto, H.; Katsube, T.; Kawamura, H.; Ouchi, C.; Iguchi, Y. Preparation of Calcium Phosphate Films by Radiofrequency Magnetron Sputtering. *Mater. Trans.* **2005**, *46*, 2246–2252. [CrossRef]
18. Lai, H.C.; Tsai, H.H.; Hung, K.Y.; Feng, H.P. Fabrication of Hydroxyapatite Targets in RF-sputtering for Surface Modification of Titanium Dental Implants. *J. Intell. Mater. Syst. Struct.* **2015**, *26*, 1050–1058. [CrossRef]

19. Hung, K.Y.; Lo, S.C.; Shih, C.S.; Yang, Y.C.; Feng, H.P.; Lin, Y.C. Titanium Surface Modified by Hydroxyapatite Coating for Dental Implants. *Surf. Coat. Technol.* **2013**, *231*, 337–345. [CrossRef]
20. Bohner, M. Calcium orthophosphates in medicine: From ceramics to calcium phosphate cements. *Injury* **2000**, *31*, 37–47. [CrossRef]
21. Ozeki, K.; Yuhta, T.; Fukui, Y.; Aoki, H. Phase composition of sputtered films from a hydroxyapatite target. *Surf. Coat. Technol.* **2002**, *160*, 54–61. [CrossRef]
22. Kweh, S.W.K.; Khor, K.A.; Cheang, P. Plasma-sprayed hydroxyapatite (HA) coatings with flame-spheroidized feedstock: Microstructure and mechanical properties. *Biomaterials* **2000**, *21*, 1223–1234. [CrossRef]
23. Lu, Y.; Li, S.; Zhu, R.; Li, M. Further studies on the effect of stand-off distance on characteristics of plasma sprayed hydroxyapatite coating. *Surf. Coat. Technol.* **2002**, *157*, 221–225. [CrossRef]
24. Schneider, S.J., Jr. *Engineered Materials Handbook, Volume 4: Ceramics and Glasses*; ASM International: Materials Park, OH, USA, 1991.
25. Heimann, R.B. Thermal spraying of biomaterials. *Surf. Coat. Technol.* **2006**, *201*, 2012–2019. [CrossRef]
26. Anil, S.; Anand, P.S.; Alghamdi, H.; Jansen, J.A. Dental Implant Surface Enhancement and Osseointegration. In *Implant Dentistry—A Rapidly Evolving Practice*; Turkyilmaz, I., Ed.; InTech: London, UK, 2011.